DEBRIS SHIELDING DEVELOPMENT FOR THE ATV INTEGRATED CARGO CARRIER

R. Destefanis[(1)], M. Lambert[(2)], F. Schäfer[(3)], G. Drolshagen[(2)], D. Francesconi[(1)]

[(1)]Alenia Spazio S.p.A., Str. Antica di Collegno 253, 10146 Turin, Italy,
rdestefa@to.alespazio.it; daniele.francesconi.aleniaspazio.it
[(2)]ESA-ESTEC, Postbus 299, NL-2200 AG Noordwijk, The Netherlands,
Michel.Lambert@esa.int, Gerhard.Drolshagen@esa.int
[(3)]Ernst-Mach-Institut – Fraunhofer fur Kurzzeitdynamik, Eckerstr. 4, D-79104, Freiburg, Germany,
Frank.Schaefer@emi.fhg.de

ABSTRACT/RESUME

The Automated Transfer Vehicle (ATV) is the European cargo spaceship that will deliver experimental equipment and spare parts as well as food, air and water to the for the International Space Station (ISS).
The meteoroids and debris protection system of the ATV has to meet stringent safety requirements related to the presence of men on board, which would be jeopardized -for instance- by a perforation of the pressurized compartment. Initially, a simple Whipple Shield with thin Aluminium bumper spaced in front of the primary structure was conceived, with a thermal Multi-layer insulation (MLI) placed on top of anti-meteoroid and debris bumper panels.
Hypervelocity impact tests - to simulate debris impacts - showed the MLI on top of the bumper shield to have an unexpectedly strong adverse influence on the ballistic performances. Several alternative configurations were tested to overcome this effect. In the end, the introduction of a light stuffing layer made of ceramic fibres and high strength aramid fabric was proved to be very efficient. The light gas gun experimental data were used to derive ballistic limit equations for the final "stuffed" shield design. These damage equations were implemented in the 3-D ESABASE/DEBRIS risk assessment tool, used to evaluate the risk posed by meteoroids and space debris to the ATV during his mission to the ISS.

1. INTRODUCTION

The Automated Transfer Vehicle (ATV) is composed by the Integrated Cargo Carrier (ICC) and the spacecraft module. The spacecraft module, after boosting the ATV into the transfer orbit, will navigate to close distance from the ISS, will perform final approach manoeuvres and fully automatic docking to the station.
The ATV ICC (shown in Figure 1) has a 45 m³-pressurised section (based on the Italian-built Multi-Purpose Logistics Module - MPLM), which is loaded with modular storage cargo elements and allows the astronauts, dressed in regular clothing, to access its contents during its joint orbital flight with ISS. The unpressurized section of the ATV ICC (External Module - EM) holds several tanks, containing up to 840 kg of drinking water, 860 kg of refuelling propellant for the Station's own propulsion system and 100 kg of air (oxygen and nitrogen).
The ATV ICC, designed and manufactured by Alenia Spazio, has a debris protection system that has to meet both stringent safety requirements and lightweight constraints intrinsic in its nature of cargo. To optimize the design, it was decided to have the thermal passive system, i.e., the Multi-layer insulation (MLI) placed on top of the Aluminium Whipple Shield bumper panels.
Hypervelocity impact tests were performed on the configurations considered during the evolution of the design phase to simulate meteoroids and debris impacts on the ATV ICC structure, firing aluminium projectiles using a Light Gas Gun (LGG). The tests lead to a proper selection of a safe configuration and allowed the evaluation of the overall ballistic performance of the shielding system.

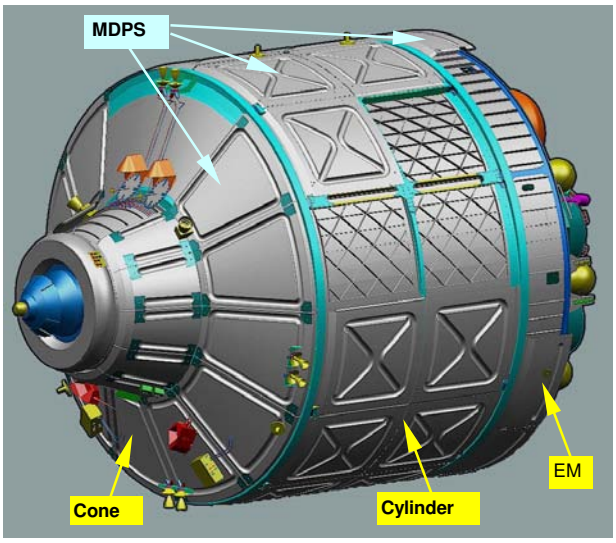

Figure 1: ATV ICC structural layout with Meteoroids and Debris Protection System (MDPS). The external MLI is not shown in figure.

2. TESTED CONFIGURATIONS

Several shielding configurations are used to protect different parts of the ATV ICC structure. The cylinder section of the ATV ICC was selected as reference configuration for debris impact testing, because of its large exposed area. LGG experiments have been performed on a few different versions of this configuration, starting from an Aluminium Whipple Shiled with only bumper and back wall (Baseline configuration). After it was decided to have the Multi-layer insulation (MLI) wrapping the external bumper, a few LGG tests were performed to assess the ballistic performance of the MLI configuration. The test results showed the MLI on top of the bumper shield to have an unexpectedly strong adverse influence on the ballistic performances. Several attempts were made to overcome this effect, while taking into account the project design constraints to keep the MLI on the external side of the shielding panels. In the end, the introduction of a light stuffing layer made of ceramic fibres and high strength aramid fabric (configuration #4 with stuffing) was proved to be very efficient to recover the required ballistic capabilities.

The decision to make the external layer of the MLI more resistant to the external environment, introducing a Teflon-coated fibre-glass woven cloth (β-cloth), requested additional testing to characterize the final flight configuration.

The generic reference configuration used for testing is depicted in Figure 2, showing all the additions considered during the test campaign (i.e., MLI, β-cloth, and the intermediate Nextel-Kevlar stuffing layers). The configurations discussed in the present paper are detailed in the following and summarized in Table 1.

#1 Baseline configuration.

It included only the following items:

- Bumper (BS) 1.2 mm Al 5083, AD: 0.315 g/cm^2
- Backwall (BW) 3.0 mm Al 2219-T851, AD: 0.852 g/cm^2

#2 MLI configuration

As the Baseline configuration plus the MLI composed of 18 layers of Double Aluminized Mylar, spaced by Dacron-net, with an external Single Aluminized Kapton layer and an internal Double Aluminized Kapton layer.

#3 β-cloth MLI configuration

As the Baseline configuration plus a β-cloth reinforced MLI. The MLI used in configuration #2 was modified replacing the external Single Aluminized Kapton with a Teflon-coated fibre-glass woven cloth.

#4 β-cloth MLI plus stuffing configuration

As the β-cloth MLI configuration plus a stuffing made from 2 layers of ceramic fabric Nextel 312 AF-10, 3 layers of Kevlar KM2 SEAL364. The Nextel/Kevlar mattress was wrapped with Single Aluminized Kapton.

Velcro straps were used to attach MLI on top of the external bumper and the Nextel-Kevlar stuffing to the rear wall, as per the flight hardware, where each Nextel/Kevlar blanket is sewed with a pattern of Velcro patches in order to provide a fixation device to the ICC shell panels. The ICC shell accommodates the mating Velcro patches by aluminium cleats bonded to the panels. The fixation device mechanical integrity was fully qualified against the thermal and mechanical environment of ATV. Note that the Nextel/Kevlar stuffing added in configuration #4 leads to a 10% increase of the areal density (excluded fixation device).

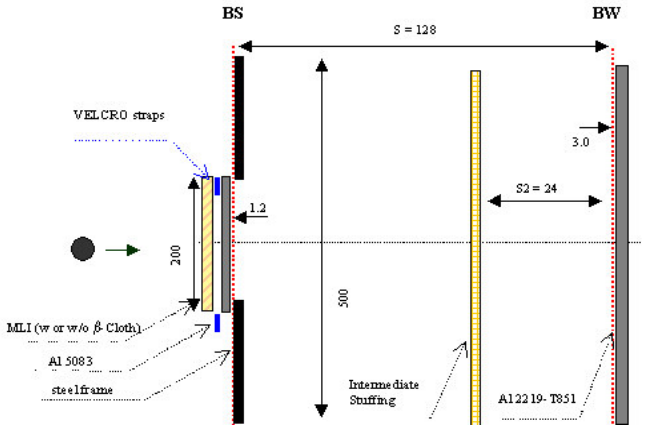

Figure 2: Layout of the ATV ICC Cylinder section generic configuration (all dimensions in mm).

Configuration	MLI AD	Stuffing AD	Total AD
#1 Baseline			1.17
#2 MLI	0.06		1.23
#3 β-cloth MLI	0.07		1.24
#4 β-cloth MLI + stuffing	0.07	0.13	1.38

Table 1: ATV ICC configurations. Area Densities (AD) in g/cm^2.

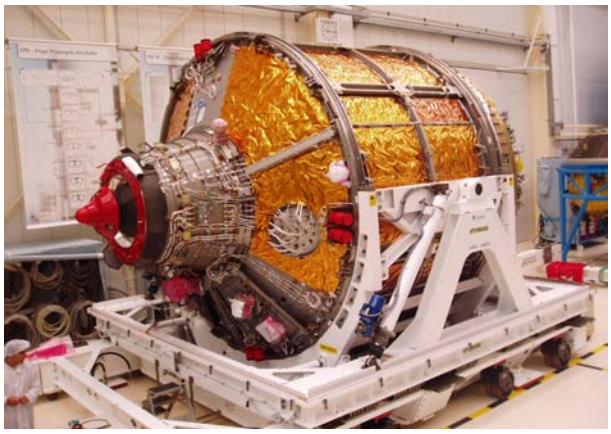

Figure 3: ATV ICC during integration activities: Kevlar Nextel stuffing blankets are attached to the shell.

3. TEST RESULTS

Hypervelocity impact tests using two-stage Light Gas Guns (Schneider, 1993) at Fraunhofer EMI (Ernst-Mach-Institut) were performed firing aluminium spheres to simulate space debris with diameters between 2.3 and 9.0 mm (0.02 and 1.07 g) at velocities comprised between 2.9 and 7.2 km/s, and with impact angles of 0, 45 and 65 degrees.

The tests results (summarized in Table 2) showed the MLI on top of the bumper shield to reduce the kinetic energy necessary to defeat the shield roughly by a factor of two (for normal impacts at about 7 km/s). The reasons for this behaviour are not yet completely understood. It is believed that the effect of the MLI is to reflect part of the shock wave at every layer, reducing the shock intensity within the projectile. This eventually leads to larger fragments hitting the rear wall and causing perforation. Figure 4 compares the test results for the baseline configuration w/o MLI (test 4053) reporting no perforation (only detached spall) under normal impact with a 6.0 mm (0.32 g) aluminium sphere at 6.7 km/s. In test 4053, the 0.5 mm thick witness plates reported a barely visible damage, indicating that the 20 x 20 mm detached spall had a limited kinetic energy. On the contrary, the MLI configuration was perforated not only by a similar projectile but also by a much smaller one (with d = 4.7 mm (0.15 g) at v = 6.9 km/s, test 4071). The different morphology of the debris cloud generated by impact against the MLI can be clearly inferred from the damage pattern on the rear wall shown in Figure 4. Also the high-speed digital shadowgraph picture taken during two similar experiments with and without MLI (see Figure 5), shows the MLI leading to a less uniformly fragmented debris cloud with a reduced radial expansion.

This MLI behaviour, leading to a lower level of projectile fragmentation and therefore higher lethality was also reported for 45° impacts. The configuration #1 w/o MLI survived a 45° impact with a 4.5 mm (0.13 g) projectile at 6.9 km/s (test 4058, no perforation, several craters), while the configuration #2 (with MLI) was penetrated by a smaller 0.42 mm (0.11 g) projectile at the same velocity (test 4057, with a 2.2 mm perforation hole surrounded by a few craters). An unexpected low ballistic limit diameter was reported for the configuration with MLI also for oblique 65° impacts, whit a perforation threshold between 4.7 mm (0.15 g, test 4062, several craters with maximum depth of 2.3) and 5.3 mm (0.22 g, test 4061, penetration hole 1.6 x 2.22 mm, surrounded by several craters) at about 6.8 km/s. When the MLI as tested in configuration #2 was modified with the introduction of an outer β-cloth layer, there were speculations that the external fibre-glass was bound to decrease the adverse MLI behaviour.

However, configuration #3 (with β-cloth reinforced MLI) did not show any improvement w.r.t. configuration #2 (MLI with external Kapton layer). On the other hand, the introduction of a light Nextel-Kevlar intermediate stuffing was sufficient not only to compensate the negative MLI effect, but to improve the final performance of the shield with a moderate mass increase. Very good ballistic performances were obtained for normal impacts both at low and high velocities. Configuration #4 survived normal impacts with diameters as large as 8.5 mm (0.9 g) at 7.15 km/s (see test 10143), with small craters (maximum depth about 0.6 mm).

The addition of the light stuffing of ceramic and aramid fabric (with a mere 10% increase of the areal density) was really effective to both reduce the lethality of the debris cloud fragments (as shown in Figure 6) and adsorb the debris cloud energy, with an increase of the ballistic limit mass by a factor of 7.

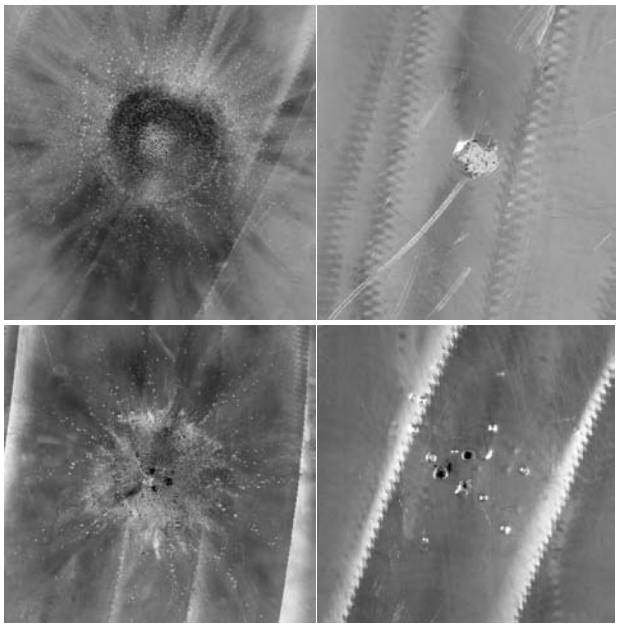

Figure 4: Above: test 4053, damage on front (left) and rear (right) of backwall. Below: test 4052, damage on front (left) and rear (right) of backwall.

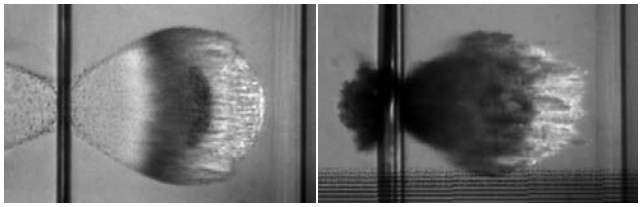

Figure 5: High-speed digital shadowgraph image of the debris cloud at 19 μs after impact. Test 4053 w/o MLI (left) and 4052 with MLI (right).

Conf. #	EMI Test No.	Projectile diameter [mm]	Projectile mass [g]	Impact velocity [km/s]	Impact angle [°]	Fail / Pass	Backwall Damage
1	4053	6.0	0.316	6.70	0	Fail	No perforation, 20x20 mm detached spall
1	4058	4.5	0.134	6.90	45	Pass	No perforation, no detached spall
2	4051	6.5	0.400	6.60	0	Fail	6 holes 1-4 mm, 2 detached spalls
2	4052	6.0	0.320	6.60	0	Fail	3 holes 2-4 mm, 6 detached spalls
2	4055	5.75	0.281	6.80	0	Fail	2 holes 1 mm, 3 detached spalls
2	4064	5.75	0.280	6.54	0	Fail	4 holes 2-3 mm, 1 hole 0.5 mm
2	4071	4.7	0.152	6.92	0	Fail	Hole size 1.2x0.8 mm, no detached spall
2	4056	4.7	0.153	6.90	45	Fail	2 holes 3 mm, no detached spall
2	4057	4.2	0.111	6.89	45	Fail	1 hole 2 mm, no detached spall
2	4061	5.3	0.222	6.78	65	Fail	1 hole 2 mm, no detached spall
2	4062	4.7	0.153	6.85	65	Pass	No perforation, no detached spall
3	10103	5.0	0.18	6.55	0	Fail	2 holes (4 and 4.5 mm diameter) out of centre
3	10105	4.5	0.13	6.55	0	Fail	1 hole (3.7 mm)
3	10107	4.5	0.13	6.60	0	Fail	2 holes (2 and 3 mm diameter) out of centre
4	4425	2.3	0.017	3.0±0.2	0	Pass	No perforation, craters <0.1 mm deep
4	4427	3.5	0.059	3.04	0	Pass	No perforation, central crater 0.34 mm deep
4	4428	4.5	0.125	3.08	0	Pass	No perforation, central crater 0.4 mm deep, small rear bulge
4	4433	5.5	Ca. 0.244	3.0	0	Pass	No perforation, small bulge on the rear side
4	4434	5.5	0.244	2.87	0	Fail	Deepest crater 2.7 mm, rear side bulge with 3.4 mm crack
4	10141	7.5	0.62	6.15	0	Pass	Deepest crater 0.55 mm deep, plate bulge 0.9 mm
4	10142	8.0	0.75	7.03	0	Pass	No perforation (hole due to LGG membrane)
4	10155	8.0	0.73	6.40	0	Pass	No perforation, deepest crater 2.0 mm, plate bulge 4.5 mm
4	10143	8.5	0.90	7.15	0	Pass	No perforation, plate bulge 8.1 mm
4	10144	7.5	0.62	6.96	45	Pass	No perforation, tiny bulge < 0.2 mm
4	10145	8.5	0.91	6.78	45	Fail	Hole size 1.9x3.7 mm, plate bulge 4.7 mm
4	10146	9.0	1.07	6.97	65	Pass	Small craters with rear side bulge (max. < 0.3 mm)

Table 2: Test results - summary. For test 10107, β-cloth and MLI located at 10 mm in front of the bumper.

Note the MLI was completely disrupted when impacted by large projectiles at high velocity and also a large delamination of the Kapton wrapping the Nextel/Kevlar stuffing was reported (see Figure 7). A significant increase of the ballistic performances was also reported under oblique impacts at high velocity.

For 45° tests, the stuffing increased the ballistic limit mass by a factor of about 6 with respect to configuration #2. At 65° the ballistic limit increased compared to the configuration w/o stuffing was by a factor of about 7.

Figure 6: Damage on front (left) and rear (right) of backwall for the configuration with stuffing (test 10143). Compare with Figure 4, bottom.

The oblique impacts at high velocity on the external bumper with MLI induced large irregular damage and bending of the front bumper.

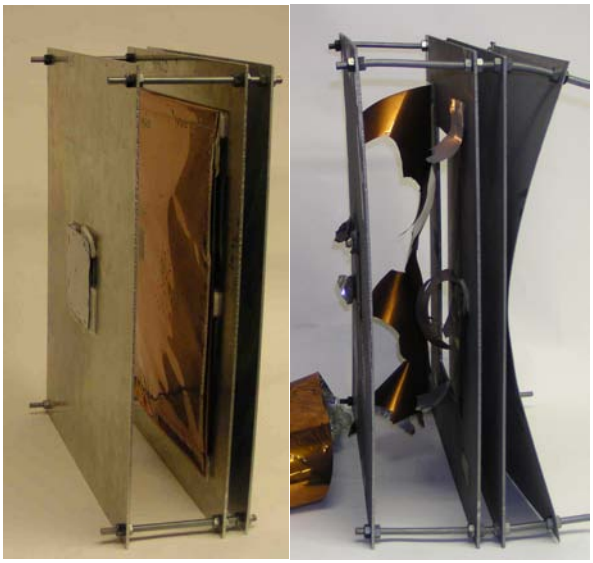

Figure 7: Target set-up before (left) and after impact (right, test 10141).

4. BALLISTIC LIMIT EQUATIONS

Ballistic limit equations (BLE) were derived (Lambert, 2003) tuning existing equations ((1) and (2), Christiansen, 1993) with the LGG impact data for the configurations tested.

- Low velocity regime (for $V_n \leq 3$ km/s):

$$d_c = \left[\frac{t_w (\sigma/40)^{1/2} + t_b}{A \cdot (\cos\theta)^{5/3} \cdot \rho_p^{1/2} \cdot V^{2/3}} \right]^{\frac{18}{19}} \quad (1)$$

- High velocity regime (for $V_n \geq 7$ km/s):

$$d_c = \left[\frac{B \cdot t_w^{2/3} (\sigma/70)^{1/3}}{(\cos\theta)^{2/3} \cdot \rho_p^{1/3} \cdot \rho_b^{1/9} \cdot V^{2/3} \cdot S^{-1/3}} \right] \quad (2)$$

Linear interpolation is used between low and high velocity regimes. The presence of MLI and/or Nextel/Kevlar stuffing has been taken into account by adding to the bumper and/or the rear wall a thickness of aluminium equivalent to the areal density of the MLI and/or stuffing, respectively. The experimental coefficients A and B of the BLE (at low and high velocity, respectively) were adjusted to fit the experimental results, as per Table 3.

The obtained BLE are compared with the LGG data in Figure 8 (projectile mass is plotted as a function of the impact velocity) for configurations #1, #2 and #4, normal and 45° impacts.

5. ATV RISK ASSESSMENT

The ESABASE/DEBRIS tool (Sdunnus, 2002) was used to quantitatively assess the impact risk for the ATV from meteoroids and debris particles. ESABASE/DEBRIS is a statistical tool to predict the number of impacts and resulting damage for user specified flux models, mission parameters, spacecraft geometry, shielding thickness and damage equation. The main results are the number of impacts from particles of a given type and size range and the Probability of No Penetration (PNP) for the specified shielding. The tool allows a 3-D analysis and fully accounts for the directional and velocity distribution of the incoming particles.

The ATV analysis was performed for a model of the ATV attached to a Russian Service Module of the ISS, shown in Figure 9, where each section of ATV with a specific shielding configuration is given a different colour and number. Different shielding types were analyzed using the damage equations described above. The final ATV shielding design consists of a β-cloth reinforced MLI plus Kevlar/Nextel stuffing shield (configuration #4) on the ATV ICC front Cone and on ¾ of the Cylinder section (the shield on the ¼ surface facing towards Earth does not have the extra stuffing, i.e., is as per configuration #3).

Configuration	A	B
#1 Baseline	0.6	3.918
#2 MLI	0.7019	2.874
#3 β-cloth MLI	0.7019	2.874
#4 β-cloth MLI + stuffing	0.315	4.945

Table 3: BLE coefficients adjusted to the experimental data.

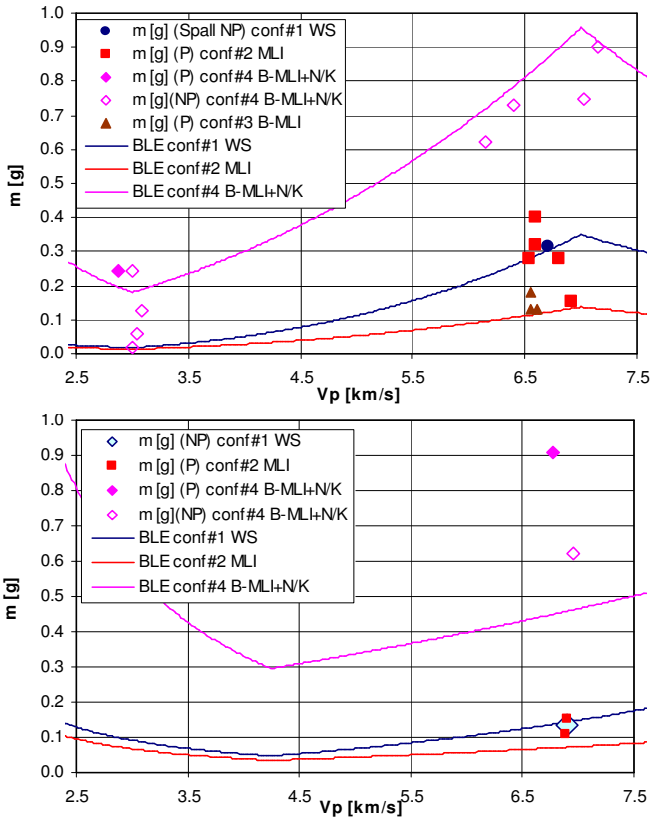

Figure 8: Test data and BLE for normal (above) and 45° (below) impacts. Empty symbols mean test passed, filled symbols mean test failed. BLE predict perforation above the curve.

All other parts of the ATV are protected by a standard Whipple Shield (mostly with β-cloth reinforced MLI, as per configuration #3). Table 4 lists the ATV sections and the corresponding shielding configurations. Note that every section is protected by a WS; the table showing only where the β-cloth MLI and/or the Nextel/Kevlar stuffing are implemented.

In most calculations it is assumed that non-conformal shields are deployed on the Russian module. The reference ISS orbit (H = 400 km, I = 51.6°) and the meteoroid and debris flux models specified in SSP 30425 (anon., 1994) are used. A slight tilt of the attitude was included (pitch: -11.2°, yaw: -6.1°). Figure 10 shows the predicted number of debris impacts /m^2/yr from particles larger than 0.1 mm displayed on the ESABASE model. The highest fluxes are encountered on the forward facing surfaces of the Russian module.

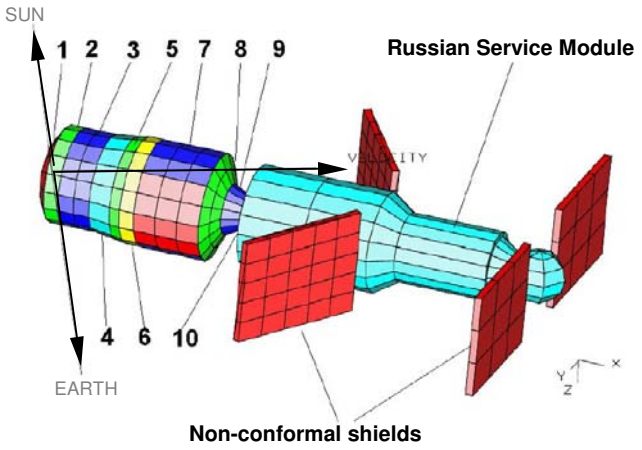

Figure 9: ATV geometry implemented in ESABASE. Different shielding systems have different colours and numbers.

No.	ATV sections	Shielding: WS +
1	ATV S/C thruster cone	β-cloth MLI
2	ATV S/C lower thruster cylinder	β-cloth MLI
3	ATV S/C upper thruster / cyl. panels	β-cloth MLI
4	ATV S/C lower avionics module	
5	ATV S/C upper avionics module	
6	ATV ICC external module	β-cloth MLI (conf #3)
7	ATV ICC pressurized cylinder	β-cloth MLI + stuffing (conf #4)
8	ATV ICC pressurized cone 2	β-cloth MLI + stuffing
9	ATV ICC pressurized cone2	β-cloth MLI

Table 4: Shielding configurations used for the various sections of ATV.

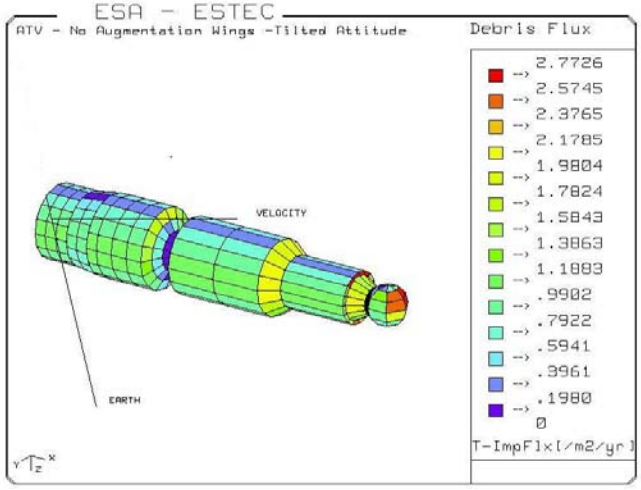

Figure 10: Predicted debris flux /m2/yr on the ATV and Russian module from space debris particles larger than 0.1mm.

However, in reality this part is shielded by other ISS modules which were not included in the analysis. The ATV will receive highest fluxes on the 'sides' and lowest fluxes on the Earth facing surfaces.

For the PNP analysis it is assumed that the non-conformal shields on the Russian module are in place. For a mission duration of 180 days and conservative analysis parameters the calculated Probability of No Penetration for the complete ATV is PNP = 0.9981.

The PNP for the pressurized module cylinder alone is 0.99975. When the data are analyzed in detail, it is seen that the overall impact risk from space debris is about 10 times larger than the risk from natural meteoroids. The added stuffing on the pressurized ATV modules provides considerable extra protection.

6. CONCLUSIONS

The design development and verification of the ATV ICC debris shielding was based on hypervelocity impact tests and ESABASE simulations. The Light Gas Gun experiments showed that placing the MLI on the external side of a Whipple Shield (with a less than 5% increase of the areal density) had an extraordinary adverse effect on the ballistic behaviour (with the projectile critical mass reduced by a factor of two). On the other hand, the incremental addition of an intermediate Nextel/Kevlar stuffing (with a 10% increase of the areal density) increased the ballistic limit mass by a factor of 7. Variations to the shielding configuration that might seem negligible may have dramatic influence on the resistance to meteoroids and debris impacts. It is therefore mandatory that the definition of the shielding configuration is not separated from the other design aspects, with a careful combination between the thermal and shielding functions. And also, when a shielding configuration is modified, hypervelocity impact tests should be performed to validate the modified ballistic capabilities.

Acknowledgements – The hypervelocity tests were performed under ESA ESTEC Contracts No. 15512/01/NL/CK and 10556/93.

7. REFERENCES

Schneider, E., Stilp, A., Meteoroid/Debris Simulation at Ernst-Mach-Institut (EMI), *Proceedings of the First European Conference on Space Debris*, Darmstadt, 1993.

Christiansen, E.L., Design and Performance Equations for Advanced Meteoroid and Debris Shields, *Int. J. Impact Engng* Vol. 14, 145-156, 1993.

Lambert M., ATV ICC Ballistic Limit Equations – Justification File, *TOS-MCS/2003/903/ln/ML*, 2003.

Sdunnus, H., Upgrade of ESABASE/DEBRIS, *Final Report of ESA contr. 15206/01/NL/ND*, *ref. R033_r024_FR,* 2002.

anon., Space Station Program Natural Environment Definition for Design, *NASA SSP 30425 Revision B*, 1994.